DOI: 10.1002/adfm.200500326

Gradient Array of Freely Suspended Nanomembranes**

By *Chaoyang Jiang*, *Dinesh S. Kommireddy*, and *Vladimir V. Tsukruk**

Freely suspended layer-by-layer nanomembranes have been transferred onto an array of circular openings of varying diameters (a gradient array). The mechanical behavior of these nanomembrane gradient arrays have been studied using both bulging tests and point-load experiments. By using the gradient array, experimental statistics are significantly improved. The observed scale-dependent mechanical properties, investigated in an efficient fashion, are evident in the trend of increasing elastic modulus with decreasing membrane diameter. The observed increase in bending rigidity with decreasing membrane diameter is satisfactorily described by the theoretical model of an elastic membrane under a point load.

1. Introduction

Layer-by-layer (LbL) assembly[1,2,3] is widely exploited for the sophisticated fabrication of multilayered structures for drug delivery,[4,5] electrochromic surfaces,[6] nanoreactors,[7] fuel cells,[8] antireflection coatings,[9] adhesive coatings,[10] and freestanding films.[11,12] In the past years, the "building blocks" for LbL assembly have been expanded into functionalized nanoparticles,[13,14] carbon nanotubes,[11,15] inorganic materials,[16] quantum dots,[17] as well as biomolecules.[18] Although conventional LbL assembly is widely applied in current studies, recently suggested spin-assisted LbL (SA-LbL) assembly[12,19] makes the assembly process more efficient. As shown in the experiments, due to the polymer-chain orientation and disentanglement, SA-LbL assembly leads to increasing stability of ultrathin multilayered films.[20] Robust, freely suspended LbL films nanoscale in thickness (below 100 nm) with record micromechanical properties and long-term stability have been recently fabricated and have been proposed as prospective sensing elements for membrane-based thermal and acoustic microsensors.[21] These nanomembranes have low flexural rigidity and extraordinarily high toughness (ultimate strength up to 100 MPa and elastic modulus of 1–10 GPa).[22,23,24] Freestanding quasi-two-dimensional (quasi-2D) polymer films with well-defined microscopic lateral shapes, which have been synthesized recently, can be exploited for these purposes.[25] Examples of patterned freestanding LbL films have been recently demonstrated for use as magnetic sensors.[26]

Integration of these compliant freestanding LbL structures into prospective microsensor arrays for acoustic or thermal sensing and imaging requires their assembly onto complex micropatterned silicon substrates with diverse surface topography (e.g., stands, posts, cavities, and trenches). One popular example of an important substrate suitable for imaging arrays is a rectangular lattice with columns and rows of circular optical cavities. Assembling nanomembranes on substrates with gradient micropatterns enables us to study their sensing behavior for potential device applications. It also provides a great opportunity to investigate the micromechanical properties of the nanomembranes with systematically varying diameters in order to elucidate their scale dependence. To the best of our knowledge, there are no reports on the successful transfer of freely suspended LbL nanomembranes onto hole arrays and the study of their micromechanical behavior under air pressure.

The goal of this study is twofold. First, we focus on assembling ultrathin (thickness about 70 nm) SA-LbL films and their careful transfer onto an array of microfabricated microscopic openings arranged in a 4×4 square pattern in a silicon substrate. We demonstrate that, in fact, robust, freely suspended 2D nanomembrane microarrays can be assembled with the transfer technology applied here and that the interference optical read-out scheme can be applied for concurrent monitoring of simultaneous deflection of 16 different circular nanomembranes under external hydrostatic pressure. To this end, we find that at any given pressure one can collect multiple independent data sets for deflecting membranes of the same diameter, thereby significantly improving experimental statistics and addressing new issues in microscopic-membrane properties. Secondly, within this rectangular array, we design columns with openings of variable diameter in order to implement a simple but efficient version of the combinatorial approach[27,28] for reliable and fast screening of nanomembrane properties under a range of conditions. This approach provides a means for concurrent study of the collective deformational behavior of membranes with four different diameters, thus addressing the question of their scale-dependent behavior.

[*] Prof. V. V. Tsukruk, Dr. C. Jiang
Department of Materials Science and Engineering
Iowa State University
Ames, IA 50011 (USA)
E-mail: vladimir@iastate.edu
D. S. Kommireddy
Institute for Micromanufacturing
Louisiana Tech University
Ruston, LA 71272 (USA)

[**] The authors thank M. E. McConney, H. Shulha, W. Y. Lio, J. Xu, and Prof. Z. Lin at Iowa State University for the experimental assistance, Dr. L. Zhang and Dr. D. Yan for the large cavity array provided, and J. Fang and Prof. Yu. M. Lvov in Louisiana Tech University for useful discussions. This work was supported by the AFOSR, F496200210205, F49620–03–1–0273, and DARPA039 AFT005 Grants.

2. Results and Discussion

Detailed descriptions of the film formation, internal microstructure, and transfer routines of similar SA-LbL films have been recently reported.[12,20,23] A layer of gold nanoparticles was encapsulated in the nanomembranes to enhance their micromechanical and optical properties (Fig. 1). The overall thickness of the membranes with gold nanoparticles sandwiched between eleven polymer multilayers on both sides (denoted as 11G11; for details, see the Experimental section) was 68 nm. The surface microroughness within an area of 1 μm × 1 μm was below 10 nm, a typical value for similar SA-LbL films with gold nanoparticles.[23] The 4 × 4 array of circular openings (holes) contained four rows of holes, with each row containing holes of a constant diameter, thus allowing for simultaneous collection of deflection data in a single run. On the other hand, four columns of holes with variable diameters (200, 100, 75, and 50 μm) allowed for concurrent monitoring of scale-dependent deflection behavior (Fig. 1). The LbL membrane transferred onto the 4 × 4 array covered all openings uniformly, as shown by the light-green color caused by light reflection by the central layer of gold nanoparticles, which have a strong surface plasmon resonance (Fig. 2a).[13a] The nanomembranes were strongly attached to the substrate and the edges of the nanomembranes could be clearly observed, as shown in Figure 2b. Optical-microscopy observation of the membranes under variable pressure showed their high stability and firm attachment to the substrate.

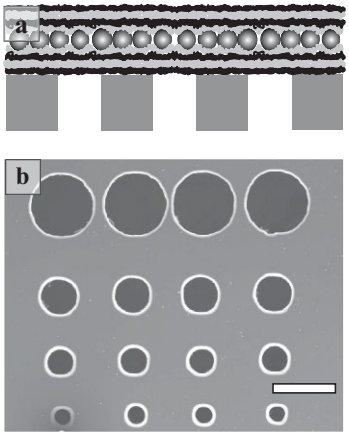

Figure 1. a) Schematic of the multilayer nanomembrane covering a hole array; b) Scanning electron microscopy (SEM) image of a silicon substrate with a gradient-diameter hole array; scale bar is 200 μm.

The membrane deflections under external pressure gradients were monitored using interference microscopy. A brief description of the home-built interferometer is given in the Experimental section, and the details have been described elsewhere.[23] The images presented in Figure 3 show the interference pattern of deflected LbL nanomembrane array under an external pressure gradient. A high pressure applied to the nanomembrane resulted in a large number of Newton's rings, indicating large out-of-plane deflections under higher pressure. Both positive and negative pressures applied to the

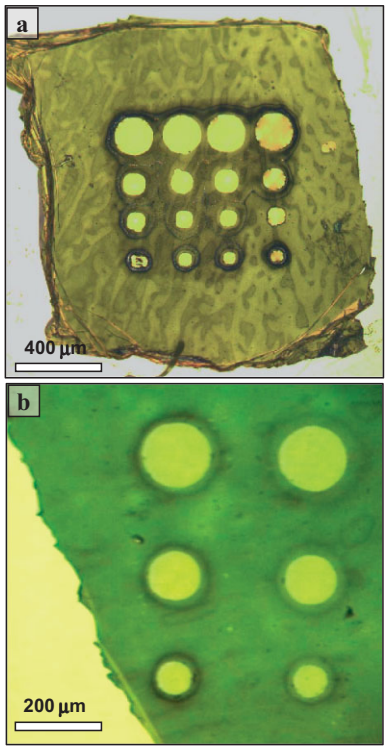

Figure 2. a) Optical image of the 4 × 4 opening array covered by the LbL membrane. b) Higher-magnification optical image of the 11G11 membrane.

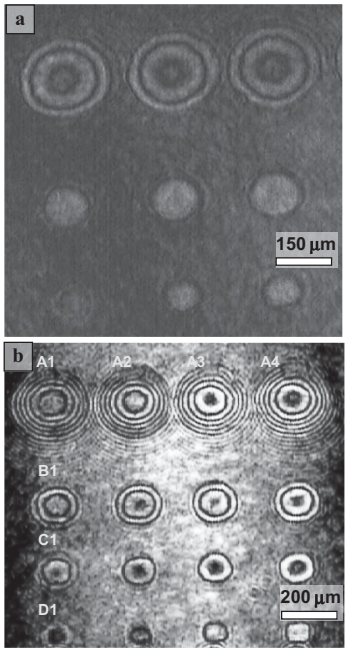

Figure 3. The interference patterns of the nanomembrane under pressure differentials of a) 525 Pa and b) 1266 Pa.

ADVANCED FUNCTIONAL MATERIALS

membrane produced similar results, as demonstrated earlier.[22] Uniform concentric Newton's rings observed for each opening were similar for all membranes with the same diameter, indicating consistent membrane deflection within the rows. However, the patterns within the columns varied significantly from top to bottom because of the variable diameter of the openings in each column (Fig. 3b). Different numbers of Newton's rings indicated different membrane deflections, as controlled by the varying diameters of the openings.[29] To achieve a detectable number of Newton's rings for the smallest openings, it was necessary to apply higher pressure, which resulted in very significant (several micrometers) deflection of the membrane suspended over the larger openings. However, due to the robustness of the nanomembranes studied here and their large dynamic ranges (deflections ranging from 1 nm to 40 μm),[20a] we seldom (less than 5 %) observed rupture of the membrane under our experimental conditions. On the other hand, the actual optical resolution of the setup used (about 5 μm in the *xy* plane) and the resolution of the charge-coupled device (CCD) camera used (5 Mpixels) limited the overall dimensions of the array which could be monitored with our optical setup to a 4×4 array, with diameters in the range 200–50 μm, and with overall dimensions of 1 mm × 1 mm. It is clear that by using the highest resolution optics available (about 1 μm for *xy* resolution) and CCD cameras with extremely high resolution (>10 Mpixels), this would allow the exploration of larger arrays with, probably, a physical limit of 10×10 cells and variations in opening diameter of 1:10.

Further quantitative analysis was facilitated by converting the interference patterns obtained under different pressures to pressure–deflection plots and deriving the elastic modulus and residual stress by applying the model of elastic-membrane deformation, as has previously been described in detail (Fig. 4a).[23] In this approach, the elastic modulus is calculated as the composite elastic modulus of the uniform membrane, representing the integrated response of the polymer–gold–polymer film. The composite elastic modulus of the membrane deposited across a 200 μm diameter opening was 5.3 ± 0.4 GPa, and the residual stress was 16.5 ± 1.5 MPa (Table 1). The elastic modulus for this membrane was slightly lower than that of the 9G9 membranes studied before because of a lower effective volume fraction of gold nanoparticles, as predicted by the mechanical models for composite materials.[20a]

Unlike previous reported measurements on a single opening, the application of the micropatterned array in this study allows the generation four independent pressure–deflection plots for four openings in a single run (Fig. 4b). This approach significantly improves the quality and statistics of measurements and allows for far more reliable determination of the elastic modulus by avoiding uncertainties related to multiple film transfers and tests under slightly different environmental conditions. In fact, the standard deviation of current measurements was within ±15 % which is much lower the typical value of ±35 % reported earlier for sequential measurements of a number of membranes fabricated and transferred at different times.[20a]

Table 1. Elastic modulus and residual stress of 11G11 nanomembranes with different diameters.

Membrane diameter [μm]	Elastic modulus [GPa]	Residual stress [MPa]
200	5.3 ± 0.4	16.5 ± 1.5
100	5.6 ± 0.2	11.7 ± 0.8
75	6.3 ± 1.0	12.5 ± 1.3
50	6.8 ± 1.2	9.3 ± 1.1

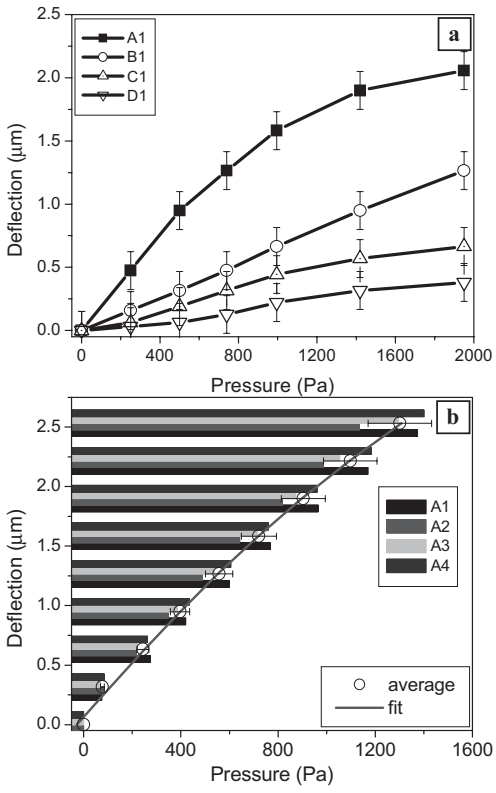

Figure 4. a) Deflection–pressure data for freely suspended nanomembranes with different diameters obtained in a single run of pressure increase; b) Four independent deflection–pressure data sets obtained simultaneously for the 200 μm freely suspended nanomembranes (four identical membranes) along with the average behavior (solid line). The labels correspond to the portions of the membranes over different openings, as shown in Figure 3b.

The systematically changing opening diameters in columns (Fig. 3) allowed us to address the question of scale dependency of the micromechanical response of compliant freely-suspended membranes, which is critical for prospective sensor arrays with variable micropatterned dimensions. Indeed, deflection–pressure data for the membranes with smaller diameters showed a consistent increase in the elastic modulus well beyond the statistical deviation. The largest elastic modulus reached 6.8 GPa for the smallest membrane, almost a 30 % increase (Table 1). Such an increase can be related to the reduced chance of having "weak" points within smaller membranes that compromise the elastic properties of the membrane. The scale-dependent elastic modulus discovered here was impossible to detect from separate measurements con-

ducted before, in which the statistical distribution was much wider.[20a] This is one of the significant advantages of the approach proposed here for studying the freely suspended nanomembrane gradient array, as opposed to single openings or uniform arrays that can be adapted for fast and efficient optimization of large arrays for high-resolution microsensors.

As an alternative method of determining the effective bending rigidity of the freely suspended membranes as a function of the membrane diameter for very small deflections (several nanometers), we applied a point-load experiment with colloidal-probe AFM (Fig. 5). Unlike deflection–pressure experiments, which exploit the membrane regime of elastic deformation with predominant tensile stress, the point-load approach, limited to very small deformations (tens of nanometers instead of micrometers), allows for studying the bending regime of the membranes and direct derivation of the bending rigidity from deflection–load data as discussed in detail before.[23] Figure 5b shows typical deflection-probe position curves generated in the course of the AFM force–distance measurements on the 11G11 nanomembrane suspended over the 200 μm diameter opening. The adhesion force was quite large for AFM tip–membrane interactions, which might be due to the relative large contact area between the 2.5 μm diameter glass microsphere and the freely suspended nanomembrane. By analyzing the experimental data, the point-load curve can be derived, as shown in Figure 5c, and the bending rigidity of freely suspended nanomembrane can be obtained by using a spring-against-spring model.

By repeating this probing of the membranes with different diameters, one can address the question of scale dependency (variation of the diameter) of the bending flexibility of the membrane. In fact, we observed a significant decrease of the maximum membrane deflection achievable under a fixed normal load for membranes with smaller diameters. The normal load of 70 nN resulted in an elastic deflection of 50 nm for the largest-diameter membrane; this deflection decreased to 37 nm for the smallest-diameter membrane (Fig. 6a). Correspondingly, the bending rigidity, B, determined directly from a simple spring-against-spring model, increased by 35 % from 1.4 $N\,m^{-1}$ to 1.9 $N\,m^{-1}$ when the membrane diameter decreased from 200 to 50 μm (Fig. 6b).

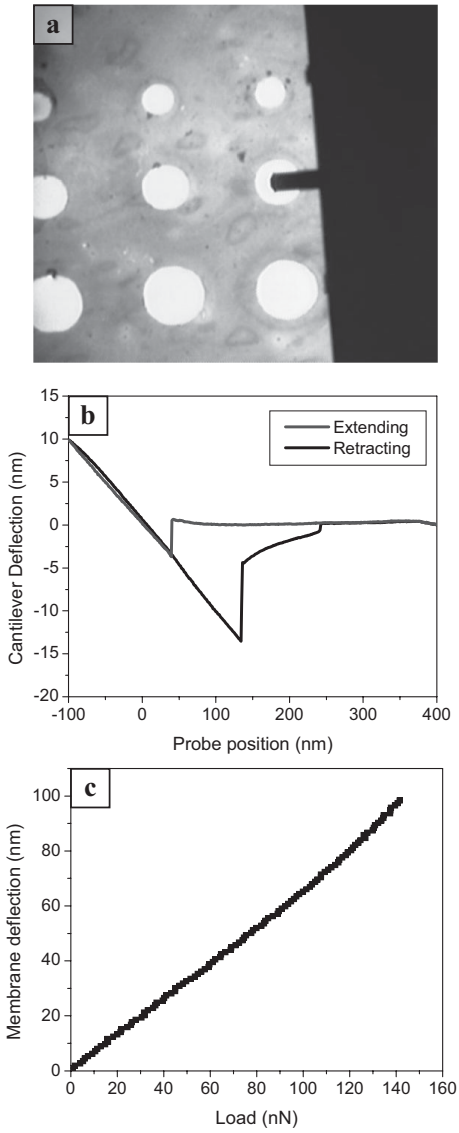

Figure 5. a) Optical micrograph of a point-load experiment with the AFM tip pointing at one of the membranes. b) Typical force–distance curve of a freely suspended membrane; the diameter of the opening is 200 μm. c) The loading curve on the membrane derived from the AFM force–distance measurement.

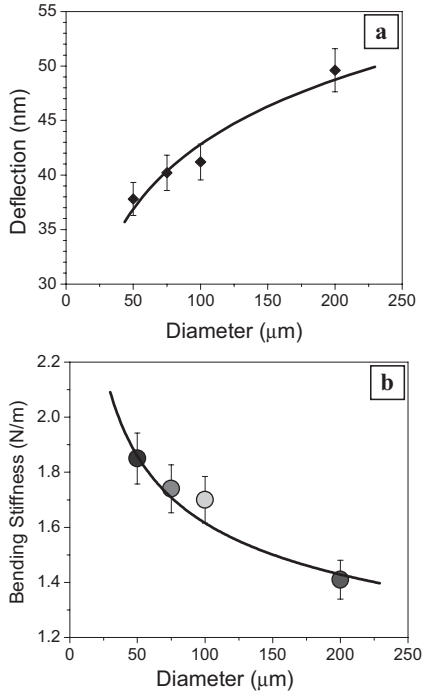

Figure 6. a) The deflection of the nanomembranes of different diameters, tested with the colloidal AFM probe under an applied force of 70 nN, as a function of the membrane diameter. b) The measured bending rigidity of the nanomembranes as a function of the membrane diameter and the theoretical prediction of elastic membrane deformation (solid line).

ADVANCED FUNCTIONAL MATERIALS

Although the increasing bending rigidity of the freely suspended membranes with decreasing diameter, D, is expected, the observed variation is very different from that predicted for uniform loads ($B \approx D^{-4}$) and from that observed earlier for larger deflections under hydrostatic pressure.[20a,30] Therefore, we analyzed this scale-dependent variation using an alternative model with a normal load applied to a small surface area.[31] This model predicts the membrane deflection under a central point load given by:

$$d(r) = \frac{P_0}{2\pi\sigma_0 h} \ln\left(\frac{R}{r}\right) \quad (1)$$

where $d(r)$ is the membrane deflection at the location a distance r away from the center, R is the radius of the opening, P_0 is the applied load, h is the film thickness, and σ_0 is the residual stress. An important result of this model is that the membrane deflection does not depend on the elastic modulus of the membrane and weakly depends upon its diameter.

Since the compliant nanomembranes studied here were extremely thin (less than 100 nm) with $h \ll D$, the bending stiffness of the membrane, which is defined as $Eh^3/12(1-\nu^2)$, where ν is the Poisson ratio, was relatively small. By fitting experimental data to the elastic deflection under a fixed normal load (Fig. 6a), a residual stress of 20 MPa was obtained for all membranes, which is close to that measured independently at larger deflections (Table 1). Moreover, from this fit, the value r, which is a characteristic of the radius of the point load, was determined to be 0.25 μm, which is close to the radius of the contact area of about 0.1 μm, as estimated using the Hertzian model for the microsphere–membrane contact.[32] Finally, by applying Equation 1 to the experimental data and assuming a residual stress of 20 MPa for all membranes, the scale-dependent bending rigidity was calculated and compared to the experimental data (Fig. 6b). As is clear, the model of the point load with realistic loading parameters describes the scale-dependent behavior of the compliant membranes with diameters decreasing from 200 to 50 μm. This model predicts the bending rigidity, B, obeys $B \approx [\ln D]^{-1}$, which is observed in our experiments and is much less dramatic than what is observed for uniform pressure loads. The theoretical simulation with finite element analysis gave similar results, as will be addressed in detail in forthcoming studies.

Finally, our preliminary experiments demonstrated that the nanomembranes studied here can be successfully transferred and freely suspended over larger opening arrays, with the number of openings reaching 192 (Fig. 7). The membrane transferred uniformly covered a 16×12 array of circular holes with a diameter of 80 μm. Figure 7 shows an image of this array with uniform nanomembrane coverage and only few defects in the lower left corner. Preliminary studies demonstrated uniform deflection of the membrane over all openings with minimum interference among adjacent cells facilitated by firm tethering of the membrane to the substrate in between the openings (about 60 μm wide). A comprehensive study of the membrane deflection on this and even larger arrays of openings (up to 64×64) with different shapes and diameters is currently in progress.

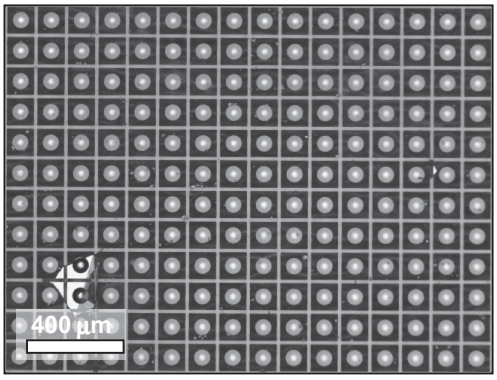

Figure 7. Large array of 192 openings (16×12) covered by the nanomembrane. The few defects in the lower left corner show the difference between the covered and uncovered area of the substrate.

3. Conclusion

We assembled freely suspended ultrathin LbL-assembled nanomembranes on the 4×4 array of openings with varying (gradient) diameters (constant in rows and variable in columns) and demonstrated its applicability for concurrent monitoring of collective deflection behavior of 16 circular nanomembranes under external hydrostatic pressure. The gradient array, designed with a variable diameter of openings in one direction, provided a means for efficient and fast screening of scale-dependent membrane properties. By using this approach, we significantly improved experimental statistics and found a modest increase in the elastic modulus with decreasing membrane diameter caused by the elimination of the weak points. Finally, we observed the scale-dependent elastic behavior with a slow, logarithmic increase of the bending rigidity with decreasing diameter of the membranes in the microscopic diameter range of 200–50 μm. This behavior is satisfactorily described by the model of the bending elastic membrane under a point load with realistic loading characteristics. We suggest that the approach introduced here can be exploited for fast and efficient screening of membrane-array properties for optimizing the sensing capabilities of thermal and pressure microsensor arrays for future demanding applications.

4. Experimental

Silicon substrates with gradient microscopic openings were fabricated using photolithography. Large squares on the back side of a 500 μm thick wafer were patterned with photoresist, developed in resist developer, and etched to a depth of 350 μm using inductively coupled plasma etching. The front side of the wafer was protected during backside etching. After etching the back side, round patterns (defining the holes to be etched) of desired diameters were patterned in the photoresist. The alignment of the front and back sides of the wafer was done during this process. These openings were then etched using inductively coupled plasma etching to create through holes in the wafer.

Freely suspended nanomembranes were fabricated with SA-LbL assembly as described earlier [12,23]. The membranes studied here contained poly(allyl amine)/sulfonated polystyrene (PAH/PSS) multilayers and a central layer containing gold nanoparticles (diameter of 12.7 nm)

[33] described as $(PAH/PSS)_{11}PAH/Gold/(PAH/PSS)_{11}PAH$ (denoted as 11G11). The membrane studied here was slightly thicker than that discussed earlier (9G9) to provide for better mechanical stability over a large area. After being released from the sacrificial cellulose acetate layer, the 11G11 membrane was picked up and placed on the silicon substrates with the microfabricated opening array (Fig. 1). The samples were kept overnight in a dessicator to allow thorough drying before mechanical testing.

The silicon substrates with nanomembranes suspended over the opening arrays were attached to a sealed chamber within an interferometric setup as described in detail elsewhere for single-opening tests [23]. Briefly, a helium–neon laser (632.8 nm) was used in this setup and the light was focused onto the sample surface. The reflected light from the surface interfered with the laser light from the reference plate, and the interference pattern was recorded by a charge-coupled device (CCD) camera. Therefore, the out-of-plane distance could be measured with a resolution of half a wavelength by counting the rings on the patterns (about 316 nm). By analysis of the interference patterns with the software, it was possible to obtain a resolution of at least a tenth of the wavelength (below 70 nm). For the bulging test [34] the pressure in the system was adjusted with a pressure pump and monitored by DPM-0.1 digital pressure module (SI Pressure Instruments Ltd, Birmingham, UK) with an accuracy of ±2 Pa. Point-load experiments were carried out on the Dimension 3000 AFM microscope (Digital Instruments) by using a colloidal-probe cantilever attached to a glass microsphere (diameter 2.5 μm) (Novascan Technology, Inc.). The spring constant of the cantilever was measured to be $14.0 \pm 2.8\ N\,m^{-1}$ using a spring-against-spring technique [35]. Scanning electron micrographs were obtained using a JSM-6060 LV microscope.

Received: May 28, 2005
Final version: July 11, 2005
Published online: November 30, 2005

[1] a) Y. Lvov, G. Decher, H. Möhwald, *Langmuir* **1993**, *9*, 481. b) G. Decher, *Science* **1997**, *277*, 1232. c) *Multilayer Thin Films* (Eds: G. Decher, J. B. Schlenoff), Wiley-VCH, Weinheim, Germany **2003**.
[2] P. T. Hammond, *Adv. Mater.* **2004**, *16*, 1271.
[3] a) V. V. Tsukruk, *Prog. Polym. Sci.* **1997**, *22*, 247. b) V. V. Tsukruk, *Adv. Mater.* **1998**, *10*, 253.
[4] a) B. Thierry, P. Kujawa, C. Tkaczyk, F. M. Winnik, L. Bilodeau, M. Tabrizian, *J. Am. Chem. Soc.* **2005**, *127*, 1626. b) B. Radt, T. A. Smith, F. Caruso, *Adv. Mater.* **2004**, *16*, 2184. c) K. C. Wood, J. Q. Boedicker, D. M. Lynn, P. T. Hammond, *Langmuir* **2005**, *21*, 1603. d) A. S. Zahr, M. de Villiers, M. V. Pishko, *Langmuir* **2005**, *21*, 403. e) F. Caruso, R. A. Caruso, H. Möhwald, *Chem. Mater.* **1999**, *11*, 3309.
[5] D. Lee, M. F. Rubner, R. E. Cohen, *Chem. Mater.* **2005**, *17*, 1099.
[6] a) D. M. DeLongchamp, P. T. Hammond, *Adv. Mater*. **2001**, *13*, 1455. b) D. M. DeLongchamp, P. T. Hammond, *Adv. Funct. Mater*. **2004**, *14*, 224.
[7] X. Shi, M. Shen, H. Möhwald, *Prog. Polym. Sci.* **2004**, *29*, 987.
[8] T. R. Farhat, P. T. Hammond, *Adv. Funct. Mater.* **2005**, *15*, 945.
[9] J. Hiller, J. D. Mendelsohn, M. F. Rubner, *Nat. Mater.* **2002**, *1*, 59.
[10] a) V. V. Tsukruk, F. Rinderspacher, V. N. Bliznyuk, *Langmuir* **1997**, *13*, 2171. b) V. N. Bliznyuk, F. Rinderspacher, V. V. Tsukruk, *Polymer* **1998**, *39*, 5249.
[11] A. A. Mamedov, N. A. Kotov, M. Prato, D. M. Guldi, J. P. Wicksted, A. Hirsch, *Nat. Mater.* **2002**, *1*, 190.
[12] C. Jiang, S. Markutsya, V. V. Tsukruk, *Adv. Mater.* **2004**, *16*, 157.
[13] a) C. Jiang, S. Markutsya, V. V. Tsukruk, *Langmuir* **2004**, *20*, 882. b) C. Jiang, S. Markutsya, H. Shulha, V. V. Tsukruk, *Adv. Mater.* **2005**, *17*, 1669.
[14] D. S. Kommireddy, A. A. Patel, T. G. Shutava, D. K. Mills, Y. M. Lvov, *J. Nanosci. Nanotechnol.* **2005**, *5*, 1069.
[15] H. Ko, C. Jiang, H. Shulha, V. V. Tsukruk, *Chem. Mater.* **2005**, *17*, 2490.
[16] Z. Tang, N. A. Kotov, S. Magonov, B. Ozturk, *Nat. Mater.* **2003**, *2*, 413.
[17] D. Zhou, A. Bruckbauer, C. Abell, D. Klenerman, D.-J. Kang, *Adv. Mater.* **2005**, *17*, 1243.
[18] a) D. G. Shchukin, G. B. Sukhorukov, H. Möhwald, *Chem. Mater.* **2003**, *15*, 3947. b) J. C. Voegel, G. Decher, P. Schaaf, *Actual. Chim.* **2003**, 30.
[19] a) J. Cho, K. Char, J.-D. Hong, K.-B. Lee, *Adv. Mater.* **2001**, *13*, 1076. b) P. A. Chiarelli, M. S. Johal, J. L. Carron, J. B. Roberts, J. M. Robinson, H.-L. Wang, *Adv. Mater.* **2001**, *13*, 1167. c) P. A. Chiarelli, M. S. Johal, D. J. Holmes, J. L. Casson, J. M. Robinson, H.-L. Wang, *Langmuir* **2002**, *18*, 168. d) V. E. Campbell, P. A. Chiarelli, S. Kaur, M. S. Johal, *Chem. Mater.* **2005**, *17,* 186.
[20] a) C. Jiang, S. Markutsya, Y. Pikus, V. V. Tsukruk, *Nat. Mater.* **2004**, *3*, 721. b) C. Jiang, W. Y. Lio, V. V. Tsukruk, *Phys. Rev. Lett.* **2005**, *95*, 115 503.
[21] A. A. Mamedov, N. A. Kotov, *Langmuir* **2000**, *16*, 5530.
[22] C. Jiang, B. M. Rybak, S. Markutsya, P. E. Kladitis, V. V. Tsukruk, *Appl. Phys. Lett.* **2005**, *86*, 121 912.
[23] S. Markutsya, C. Jiang, Y. Pikus, V. V. Tsukruk, *Adv. Funct. Mater.* **2005**, *15*, 771.
[24] a) A. Fery, F. Dubreuil, H. Möhwald, *New J. Phys.* **2004**, *6*, 18. b) O. I. Vinogradova, *J. Phys.: Condens. Matter* **2004**, *16,* R1105.
[25] A. D. Stroock, R. S. Kane, M. Weck, S. J. Metallo, G. M. Whitesides, *Langmuir* **2003**, *19*, 2466.
[26] F. Hua, T. Cui, Y. Lvov, *Nano Lett.* **2004**, *4*, 823.
[27] a) K. Ashley, J. C. Meredith, D. Raghavan, E. J. Amis, A. Karim, *Polymer* **2003**, *44*, 769. b) A. P. Smith, J. F. Douglas, J. C. Meredith, E. J. Amis, A. Karim, *Phys. Rev. Lett.* **2001**, *87*, 015 503.
[28] R. Song, M. Y. M. Chiang, A. J. Crosby, A. Karim, E. J. Amis, N. Eidelman, *Polymer* **2005**, *46*, 1643.
[29] C. Poilane, P. Delobelle, C. Lexcellent, S. Hayashi, H. Tobushi, *Thin Solid Films* **2000**, *379*, 156.
[30] J. W. Beams, in *Structure and Properties of Thin Solid Films* (Eds: C. A. Neugebauer, J. B. Newkirk, D. A. Vermilyea), John Wiley, New York **1959**.
[31] N. Tang, R. L. Engelstad, E. G. Lovell, *Microelectron. Eng.* **2002**, *61–62*, 271.
[32] K. L. Johnson, *Contact Mechanics*, Cambridge University Press, Cambridge, UK **1985**.
[33] K. C. Grabar, R. G. Freeman, M. B. Hommer, M. J. Natan, *Anal. Chem.* **1995**, *67*, 735.
[34] J. J. Vlasak, W. D. Nix, *J. Mater. Res.* **1992**, *7*, 3242.
[35] a) J. L. Hazel, V. V. Tsukruk, *J. Tribol.* **1998**, *120*, 814. b) J. L. Hazel, V. V. Tsukruk, *Thin Solid Films* **1999**, *339*, 249.